Superconductivity, magnetic susceptibility, and electronic properties of amorphous $(Mo_{1-x}Ru_x)_{80}P_{20}$ alloys obtained by liquid quenching

W. L. Johnson, S. J. Poon,* J. Durand,† and P. Duwez
W. M. Keck Laboratory of Engineering Materials, California Institute of Technology, Pasadena, California 91125
(Received 13 December 1977)

Results of x-ray diffraction, transmission-electron diffraction, and crystallization studies on amorphous $(Mo_{1-x}Ru_x)_{80}P_{20}$ alloys obtained by liquid quenching are presented and discussed. The alloys are all found to be superconducting with transition temperatures ranging from ~ 3 to ~ 9°K. The variation of T_c with alloy composition is compared to that obtained by Collver and Hammond for vapor-quenched transition-metal films. Results of magnetic-susceptibility measurements are used to estimate the variation of the electronic density of states at the Fermi level $N(0)$ from the Pauli paramagnetic contribution. The relationship between the variation of T_c and $N(0)$ is discussed in terms of the microscope theory of superconductivity. Finally, results of measurements of the upper critical field H_{c2}, and the normal-state electronic transport properties are presented and compared with recent theoretical models for amorphous superconductors.

I. INTRODUCTION

Since the early work of Buckel and Hilsch,[1,2] interest in the study of amorphous superconducting metals and alloys has steadily increased. A review of experimental and theoretical work in this area has been published by Bergmann.[3] To date most experimental results have concerned thin films obtained by vapor deposition on a cryogenic substrate, as amorphous superconducting metals and alloys were until recently not available in bulk form. The authors have reported superconductivity in bulk amorphous alloys obtained by the method of liquid quenching.[4] These amorphous alloys are stable with respect to crystallization at and well above room temperature. Owing to this stability and to the relatively large quantity of sample available, it is possible to carry out measurements of bulk properties such as specific heat[5] and magnetic susceptibility on these materials.

The transition metals and their alloys form a particularly interesting class of superconducting materials. Collver and Hammond,[6] have shown that it is possible to obtain transition metals in amorphous form by vapor deposition on a substrate held at 4.2 °K. For transition metals of a given series and alloys of neighboring metals in the series, they observed that the superconducting transition temperature T_c follows a regular dependence on d-band occupation or average group number (AGN). A broad maximum in the T_c vs AGN curve with the maximum occurring at an AGN corresponding to a roughly half-filled d band was found. This behavior is in marked contrast to the double-peaked structure characteristic of crystalline alloys which is commonly referred to as the Matthias rule. The microscopic origin of the variation of T_c in the amorphous state and its contrast to the crystalline case has been the subject of several subsequent studies.[7-9] Unfortunately, attempts to understand this problem have suffered from a lack of detailed information regarding the variation of fundamental microscopic parameters in the amorphous state. Experimental data regarding the electronic band structure and density of states at the Fermi level, $N(0)$, are not available. The variation of the Debye temperature and phonon density of states have likewise not been studied. Such information is essential to explaining the microscopic origin of the systematics of T_c.

In the present work, we report on the properties of several new amorphous transition-metal alloys prepared in bulk form using the liquid-quenching technique. The alloys contain 80 at.% of a transition metal and 20 at.% of a "glass forming" constituent such as phosphorus or boron. Together, they form an alloy series in which the d-band occupation is varied systematically. The variation of T_c is found to closely follow that observed by Collver and Hammond. Deviations observed are attributed to the effects of electron transfer from the transition-metal constituent to the more electronegative glass-forming constituent. Magnetic-susceptibility measurements carried out over the temperature range from 2 °K to room temperature and for fields ranging up to 80 kG are used to evaluate the temperature-independent magnetic susceptibility. These data enable one to estimate the variation of $N(0)$ with d-band occupation for the alloy series provided that it is assumed that the Pauli paramagnetic susceptibility is the dominant contribution to the temperature-independent part. By making this approximation, and neglecting many-body effects, approximate values of $N(0)$

have been obtained. The values of $N(0)$ are found to vary smoothly with d-band occupation and this variation can be correlated with the variation in T_c for the alloy series. The microscopic theory of superconductivity is used together with the present data to interpret the systematics of transition-metal superconductivity in the amorphous state. A tight-binding model for electronic structure of the d band originally proposed by Labbé, Barasic, and Friedel[10] and modified by Varma and Dynes[11] to include nonorthogonality of the basic functions is compared with the experimental data.

Several other properties of this series of alloys have been measured. Structural data obtained both from electron diffraction and x-ray diffraction are discussed. High-temperature-resistivity data and thermal-scanning data are presented which together with the structural data support the claim that the alloys are amorphous. The temperature dependence of the upper critical field $H_{c2}(T)$, and the field gradient $dH_{c2}(T)/dT$ have been measured for all alloys of the series. These data are compared to theoretical predictions. Finally, the factors which govern the formation of the amorphous phase and its stability are analyzed and related to the present results.

II. EXPERIMENTAL

The alloy preparation is accomplished in several steps using 99.9% and 99.99% pure starting materials. Metal powders are combined and thoroughly mixed with phosphorous and boron powders then pressed to form a compact. The compact is sealed in quartz and slowly heated to ~1100 °C over a period of several days. The reacted compact is melted several times on a silver boat under an argon atmosphere to form a homogeneous ingot. The ingot is subsequently broken into small fragments which are used in the liquid-quenching process. The quenching technique is described elsewhere.[12] The quenched samples are in the form of foils having a typical thickness of ~60 μm and an area of several cm^2.

All samples are checked by x-ray diffraction scanning with a Norelco diffractometer using Cu $K\alpha$ radiation. A time lapse step scanning diffractometer was also used to obtain a more detailed x-ray scan with improved statistics. Several foils were thinned by etching and used for electron diffraction studies in a Siemens transmission electron microscope.

Electrical resistivity measurements were carried out at two stations one of which can be used for temperatures in the range from 4.2–300 °K, and a second for temperatures in the range from 300–1200 °K. Thermal traces were obtained by rapid heating in an evacuated tube with a platinum-platinum rhodium thermocouple attached to the sample foil.

Magnetic-susceptibility measurements were carried out using the Faraday method in a superconducting magnet system designed by Oxford Instruments. The fields used range up to 80 kG and the sample temperature can be controlled in the range from 2–300 °K. Measurements of $H_{c2}(T)$ were carried out in the same system using a separate probe. The sample is located in an exchange gas container and can be mounted in three mutually orthogonal directions. Below 10 °K, the temperature can be measured with an absolute accuracy of ±50 mK and a relative accuracy of ±1 mK. The $H_{c2}(T)$ data were obtained by measuring resistance versus temperature curves for a series of constant applied fields. Critical current as a function of applied field and temperature was also measured. Transition temperatures reported are defined as the highest temperature for which the resistivity $\rho = 0$ in zero applied field. The transition temperatures were also measured using an ac induction bridge (at a separate station). The T_c values obtained by the two techniques are in good agreement (a maximum discrepancy of ±0.1 °K is observed). A list of all alloy compositions studied

TABLE 1. Transition temperature, critical-field gradient, and resistivity of amorphous superconducting alloys prepared by liquid quenching.

Alloy composition	T_c (°K)	dH_{c2}/dT (kG/°K)	Resistivity[a] ($\mu\Omega$ cm)
$(Mo_{0.8}Ru_{0.2})_{80}P_{20}$	7.31 ± 0.05	24.5 ± 0.5	300 ± 50
$(Mo_{0.6}Ru_{0.4})_{80}P_{20}$	6.18 ± 0.05	25.5 ± 0.5	300 ± 50
$(Mo_{0.4}Ru_{0.6})_{80}P_{20}$	4.68 ± 0.05	26.8 ± 0.5	330 ± 50
$(Mo_{0.2}Ru_{0.8})_{80}P_{20}$	3.43 ± 0.05	27.6 ± 0.5	320 ± 50
$Mo_{80}P_{10}B_{10}$	9.00 ± 0.05	17.6 ± 0.5	...
$(Mo_{0.8}Re_{0.2})_{80}P_{10}B_{10}$	8.71 ± 0.05	24.2 ± 0.5	...

[a] Room temperature.

along with the T_c observed at each composition is given in Table I. The T_c values in the table are an average over at least three samples with the nominal composition. For a given nominal composition, T_c varies by no more than ±0.1 °K among samples. Also given in Table I are values of the electrical resistivity and upper critical-field gradient for each alloy composition. Again, these data are averaged over several samples.

III. RESULTS AND COMPARISON WITH PREVIOUS WORK

A. Structure and crystallization

The x-ray scattering intensity as a function of scattering angle for amorphous $(Mo_{1-x}Ru_x)_{80}P_{20}$ alloys can be compared to that observed for several other amorphous transition-metal alloys containing phosphorus. An example of data obtained by time lapse step scanning is shown in Fig. 1 for $(Mo_{0.6}Ru_{0.4})_{80}P_{20}$. Three broad maxima with successively decreasing amplitude are observed in the x-ray intensity as a function of scattering angle 2Θ. It was not possible using Cu $K\alpha$ radiation to reach sufficient values of the scattering vector to investigate a fourth possible maximum. Rising background near the third maximum is due to Compton scattering. Particularly interesting features in Fig. 1 include the pronounced shoulder on the second maximum, the height and width of the successive maxima, and the positions of the maxima. These features are very similar to those observed by Cargill and Cochrane[13,14] for $Ni_{76}P_{24}$ and $Co_{78}P_{22}$ amorphous alloys, and by Wagner[15] for amorphous $Fe_{80}P_{13}C_7$ alloys. The splitting of the second maximum in the present data was observed for each of the above alloys. The widths of the first, second, and third maxima are also comparable to those observed in the above mentioned work. It

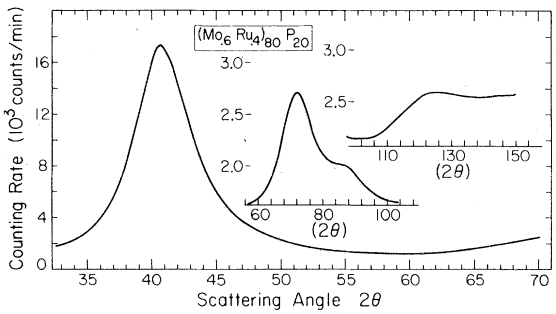

FIG. 1. X-ray scattering intensity as a function of scattering angle (2Θ) for amorphous $(Mo_{0.6}Ru_{0.4})_{80}P_{20}$. The intensity function is obtained by step scanning at angular intervals of $\Delta(2\Theta) = 0.1°$. A continuous line is presented as the data points are too densely dispersed to be distinguished.

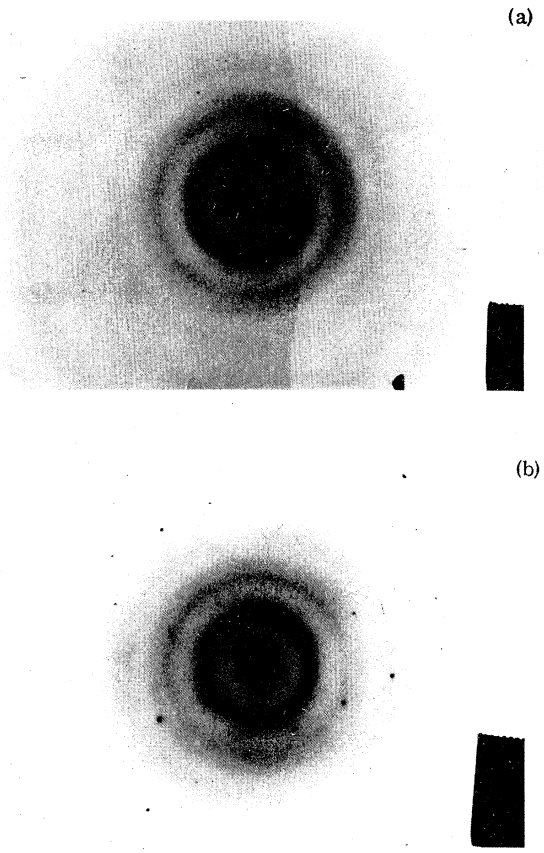

FIG. 2. (a) Transmission-electron diffraction pattern for a typical region of an amorphous $(Mo_{0.6}Ru_{0.4})_{80}P_{20}$ sample. The foil was thinned by chemical etching; (b) Transmission-electron diffraction pattern of a region of a $(Mo_{0.2}Ru_{0.8})_{80}P_{20}$ specimen containing a microcrystallite embedded in an amorphous matrix. Most regions of this sample showed no evidence of crystallization.

should be noted that, according to the Scherrer formula, the width of the first maximum corresponds to an effective microcrystal size of about 16 Å. Although the radial distribution function (RDF) has not yet been calculated for the present alloys, it is probable that the general features will resemble those obtained by Cargill and Cochrane, and Wagner. Their data were found to be well described by theoretical models for amorphous structure.[13-15]

Electron diffraction studies of amorphous $(Mo_{1-x}Ru_x)_{80}P_{20}$ alloys also support the conclusion that they possess an amorphous structure. The transmission electron diffraction pattern of an $(Mo_{0.6}Ru_{0.4})_{80}P_{20}$ sample which was thinned by chemical etching is shown in Fig. 2(a). Three diffuse halos are visible and a fourth can be seen on close inspection. Electron diffraction patterns of

other alloys of the $(Mo_{1-x}Ru_x)_{80}P_{20}$ series are similar. A few isolated regions of an $(Mo_{0.2}Ru_{0.8})_{80}P_{20}$ specimen were found to give diffuse halos plus spots indicating that microcrystallites had formed in the amorphous matrix during quenching. An example is shown in Fig. 2(b). This composition must lie near the upper limit of Ru concentrations for which it is possible to obtain an amorphous phase by liquid quenching. It was not possible to obtain amorphous samples of $Mo_{80}P_{20}$ which indicates that a lower limit for Ru concentration also exists.

The crystallization of amorphous $(Mo_{1-x}Ru_x)_{80}P_{20}$ alloys was studied both by measurement of high-temperature resistivity and by carrying out a thermal trace. The resistivity versus temperature for $(Mo_{0.6}Ru_{0.4})_{80}P_{20}$ obtained using a heating rate of 5 °K/min is shown in Fig. 3(a). The data spans the range from 4.2–1200 °K (the superconducting transition at ~6.1 °K is not shown). The resistivity exhibits a negative temperature coefficient $(1/\rho)(d\rho/dT)$ over the temperature range up to ~600 °K. The resistivity is observed to drop abruptly at about 980 °K. This precipitous drop is taken to indicate spontaneous crystallization of the alloy. Such a drop provides additional evidence of a well-defined amorphous state. It should also be noted that further heating to 1200 °C results in a subsequent cooling curve having a positive coefficient of resistivity as expected for a crystalline material.

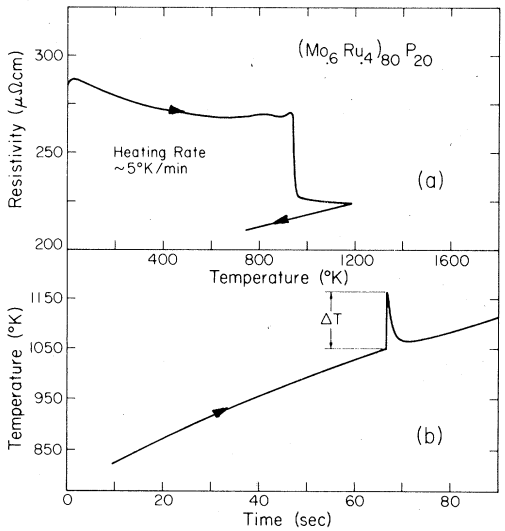

FIG. 3. (a) Electrical resistivity of an amorphous $(Mo_{0.6}Ru_{0.4})_{80}P_{20}$ sample from low temperature up to 1200 °C. The sample was heated at a rate of 5 °K/min; (b) Thermal trace of an amorphous $(Mo_{0.6}Ru_{0.4})_{80}P_{20}$ sample obtained by rapidly heating the sample with attached thermocouple in an evacuated quartz tube. Crystallization is accompanied by a sharp temperature rise ΔT indicated on the plot.

The thermal trace was obtained by heating the sample at a rate of ~5 °K/sec. The sample is sealed in an evacuated quartz tube and plunged into a preheated furnace. The sample temperature as monitored by an attached thermocouple is recorded as a function of time. The results are shown in Fig. 3(b). A sharp rise in temperature is observed at 1040 °K. The temperature rise ΔT is ~120 °K. This value can be used to obtain a lower bound (the measurement is not strictly adiabatic) for the heat of crystallization of the amorphous phase. Since the temperature involved must be several times the Debye temperature of the alloy, the Dulong-Petit value of $3R$ for the heat capacity can be used. The heat of crystallization ΔH_c is then given by $3R\Delta T$. This gives $\Delta H_c \geq 0.72$ (kcal/mole). The melting point of $(Mo_{0.6}Ru_{0.4})_{80}P_{20}$ can be roughly estimated from the liquid-quenching procedure to be of order 1800 °K and the heat of fusion ΔH_F will thus be of the order of several (kcal/mole). ΔH_c represents a significant fraction of ΔH_F as would be expected if the alloy is initially in the amorphous state. Thermal trace data were taken on other alloys of the $(Mo_{1-x}Ru_x)_{80}P_{20}$. All alloys of the series show an abrupt temperature increase which occurs at a temperature between 1000 °K and 1080 °K. The $Mo_{80}P_{10}B_{10}$ and $Mo_{60}Re_{20}P_{16}B_{10}$ alloys crystallize at ~1100 °K as measured by the thermal trace using the same heating rate.

The discrepancy between the crystallization temperature obtained from resistivity versus temperature and that obtained from the thermal trace data can be attributed to the difference in the heating rates used in the two cases. The faster heating rate in the thermal trace allows a much shorter time lapse per unit of temperature scanned and thus a smaller time interval in which nucleation of the crystalline phase can take place.

B. Superconductivity

The superconducting transition temperature T_c for each of the alloys is listed in Table I. T_c was found to be a systematic function of the AGN of the transition-metal component where the AGN of Mo and Ru are six and eight, respectively. This dependence is illustrated in Fig. 4. For comparison, the dependence of T_c on AGN observed by Coliver and Hammond[6] for Mo-Ru alloys prepared by vapor quenching on a cryogenic substrate is shown. The general features of the two curves are similar although some differences are apparent. The peak in T_c vs AGN curve occurs at somewhat lower AGN than that obtained by Collver and

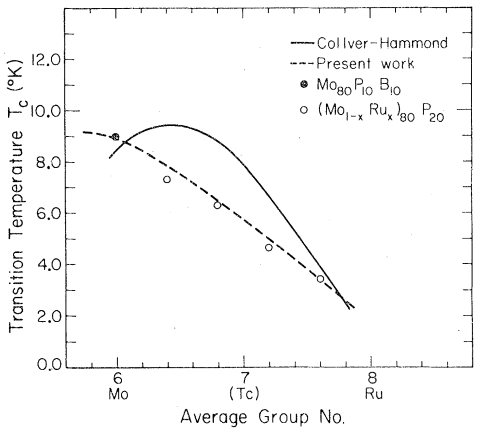

FIG. 4. Superconducting transition temperature as a function of the AGN of the transition-metal constituent for amorphous $(Mo_{1-x}Ru_x)_{80}P_{20}$ alloys and an $Mo_{80}P_{10}B_{10}$ alloy. The dashed line indicates the trend of the present experimental data while the solid line exhibits the behavior observed by Collver and Hammond for cryo-quenched transition-metal films.

Hammond. The two curves join for AGN values near eight. Otto Meyer[16,17] has pointed out that the T_c of transition-metal films ion implanted with group A elements at low-temperature approach those given by the Collver-Hammond curve for sufficiently high dosages of implanted ions and provided that the electronegativity and Goldschmidt radii of the implanted species fall in a certain range. Meyer's work suggests that chemical factors play a role in determining T_c. In the present work, the phosphorus (and boron for some of the alloys) atoms probably interact chemically with the transition-metal species. The Pauling electronegativities of Mo, Ru, and P are 1.8, 2.2, and 2.1, respectively. Some electron transfer from Mo to P is expected while little or no transfer is expected from Ru to P. Transfer of an electron having a predominantly s-like character from Mo to P would result in a lowering of the Mo atomic d level due to the increase of charge on the Mo site. A net relative increase in d-band occupation could result. Electron transfer probably does not occur for Ru since the electronegativity difference between Ru and P is of opposite sign and small. Such considerations may underlie the apparent discrepancy in the T_c vs AGN curve (Fig. 4) with respect to that of Collver-Hammond. A shift occurs for the Mo-rich alloys but not for Ru-rich alloys as expected.

The superconducting transition as measured by resistance versus temperature for amorphous $(Mo_{0.6}Ru_{0.4})_{80}P_{20}$ is shown in Fig. 5 for the case of no applied magnetic field ($H=0$) along with transition in various nonzero fields. For $H=0$ the width of the superconducting transition $\Delta T_c \simeq 40\times10^{-3}$ °K as measured by the 10% and 90% points on the resistance versus temperature curve. This value of ΔT_c is comparable to that observed in numerous other amorphous samples.[4,18,19] The rounding of the resistive transition above T_c has been shown to be due to superconducting fluctuations and is also discussed elsewhere.[18,19] Broadening of the superconducting transition in the presence of an applied field has also been discussed in the above references and is probably attributable to the effect of surface superconductivity. The resistive transitions for other alloys studied are very similar to that shown in Fig. 5.

The upper critical field H_{c2} and its temperature dependence can be defined in terms of the curves in Fig. 5. Taking the temperature for which the resistance is $\frac{1}{2}$ of the normal-state value for a given applied field defines the temperature-dependent upper critical field. One could adopt other criteria such as $R=0$ in defining the upper critical field. Using the $R=0$ criteria will give a slightly reduced field gradient (dH_{c2}/dT) but does not significantly alter the functional dependence obtained for H_{c2} on temperature. The $H_{c2}(T)$ data for $(Mo_{0.6}Ru_{0.4})_{80}P_{20}$ are shown in Fig. 6 along with those of all alloys studied. In all cases, H_{c2}, is well described by the formula

$$H_{c2}(T)=(1-T/T_c)H_{c2}(0)\,, \qquad (1)$$

where $H_{c2}(0)$ is defined by linear extrapolation of

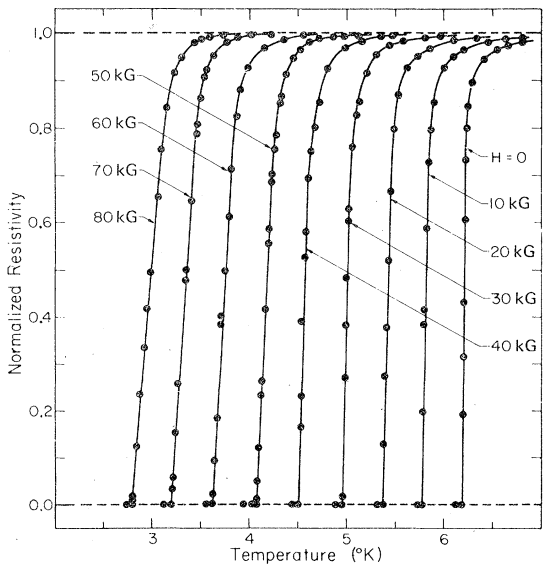

FIG. 5. The normalized resistivity $[\rho(T)/\rho(10\,°\mathrm{K})]$ of amorphous $(Mo_{0.6}Ru_{0.4})_{80}P_{20}$ as a function of temperature in the presence of a transverse magnetic field. The field ranges from $H=0$ to $H=80$ kG.

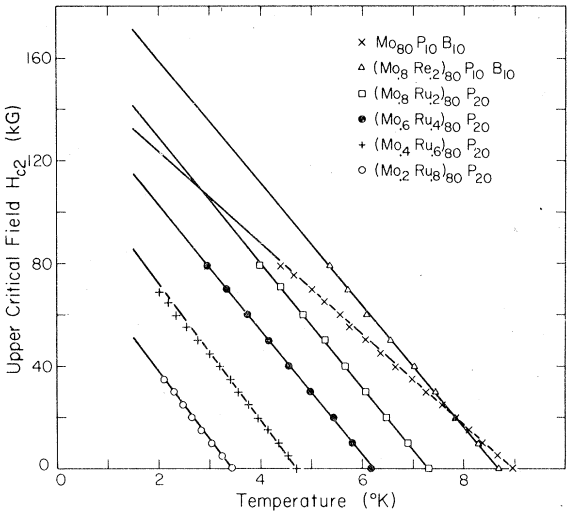

FIG. 6. Upper critical field $H_{c2}(T)$ as a function of temperature for all of the amorphous alloys of the present study. The values of $H_{c2}(T)$ were determined by the $R=\frac{1}{2}R_0$ criteria described in the text.

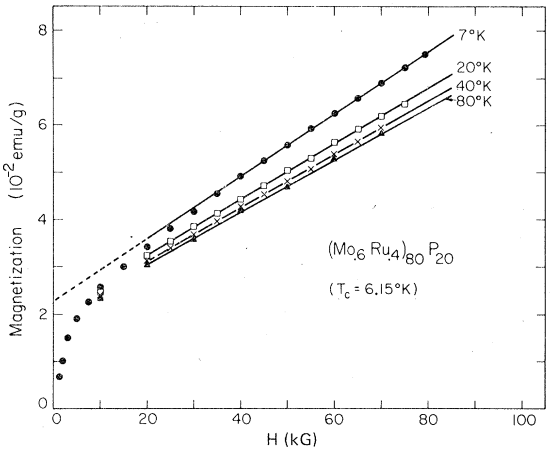

FIG. 7. Magnetization as a function of applied field H for amorphous $(Mo_{0.6}Ru_{0.4})_{80}P_{20}$ for various temperatures as indicated on the graph. The solid lines were used to determine $\chi(T)$, the temperature-dependent magnetic susceptibility of the amorphous matrix.

the data to $T=0$. Within experimental error, little deviation from linearity is observed for the $H_{c2}(T)$ curves over the range of fields and temperatures available. For several of the alloys, this range covers over half of the total range of reduced temperature $t=T/T_c$. Previous studies of amorphous transition-metal alloys have also given a linear $H_{c2}(T)$ is dependence.[4,20-22] Deviations from linearity have been observed for amorphous V and $Zr_{75}Rh_{25}$,[19,23] but are not as large as those predicted by the Maki theory[24] even when spin-orbit coupling and paramagnetic limiting are included.

Critical current-density measurements in both zero and nonzero applied magnetic field have also been carried out for most of the alloys. For $H=0$ typical values of J_c range from 5×10^4 to 3×10^5 A/cm^2 for high-T_c and low-T_c alloys, respectively. Weak flux pinning forces are observed in some alloys. The flux pinning profiles and other data relating to flux pinning will be discussed in a separate publication.[25]

C. Magnetic measurements

Magnetization M as a function of applied field was measured for each of the alloys. Data were taken for a series of fixed temperatures by varying the applied field of H. The magnetization in both the normal and superconducting state was studied. The data taken for temperatures above T_c were used to determine the temperature and composition dependence of the normal-state magnetic susceptibility. A typical set of data is shown in Fig. 7 for amorphous $(Mo_{0.6}Ru_{0.4})_{80}P_{20}$. The T_c of the alloy is 6.15 °K so that all of the data shown were taken in the normal state. The sharp rise in magnetization for $H<10$ kG arises from contamination of the sample during laboratory handling and cutting by particles of Fe (or other magnetic materials). This contribution changes only slightly with temperature and is therefore not due to magnetic impurity atoms dissolved in the matrix. A very small temperature-dependent term corresponding to such impurities is present. The magnetization due to such contamination is well saturated at $H=20$ kG so that the change in magnetization above 20 kG is governed by the susceptibility $\chi(T)$ of the amorphous matrix. From 20 to 80 kG, the M vs H curve is linear and $\chi(T)$ is well defined. For low temperatures (7–20 °K), $\chi(T)$ shows a temperature dependence. The data taken at 40 °K and 80 °K are nearly identical. A well-defined temperature-independent contribution to $\chi(T)$ can thus be defined by the high-temperature data. Similar results were obtained for other alloys of the $(Mo_{1-x}Ru_x)_{80}P_{20}$ series. A summary of the temperature-independent part of $\chi(T)$ defined by data taken at 80 °K (or higher when necessary to establish temperature independence) and referred to as χ is presented in Fig. 8(a). In Fig. 8(b) the susceptibility has been converted to units of (states/eV atom) for later convenience by plotting the quantity $\chi/2\mu_B^2$ where μ_B is the Bohr magneton. It can be seen that χ follows a regular dependence on the AGN of the transition-metal constituents. The variation is similar to that observed for T_c vs AGN; this correlation will be discussed at length in Sec. IV. Previous measurements on other amorphous transition-metal–phosphorus alloys with

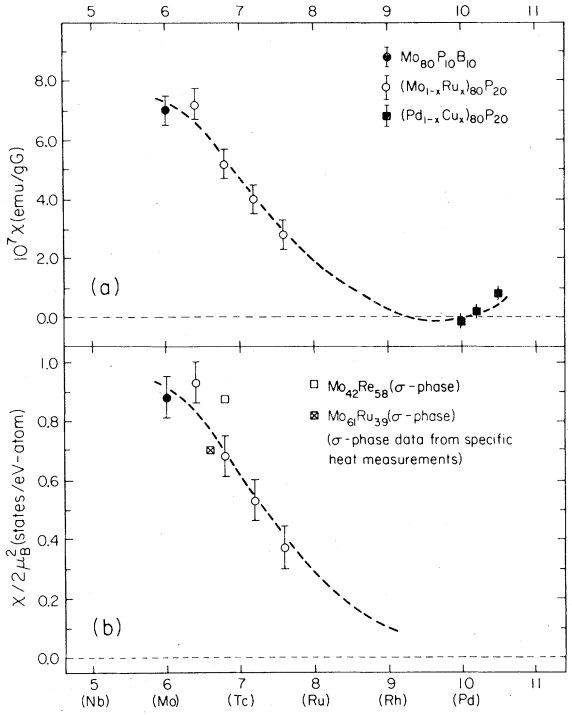

FIG. 8. (a) Temperature-independent part χ of the magnetic susceptibility $\chi(T)$ (defined by high-temperature magnetization data) for the amorphous alloys of this study. Also shown are data for amorphous $(Pd_{1-x}Cu_x)_{80}P_{20}$ alloys taken from a previous study [G. Tangonan, Ph. D. thesis (California Institute of Technology, 1976 unpublished)]. The data are plotted as a function of AGN for the transition-metal constituents. (b) Density of states ($\chi/2\mu_B^2$) obtained from the magnetic susceptibility shown in (a). The electron density of states at the Fermi level $N(0)$ for crystalling σ phase Mo-Re and Mo-Ru alloys as determined from low-temperature specific-heat data is also shown for comparison with the values of $\chi/2\mu_B^2$ obtained for the amorphous alloys.

higher AGN values give values of χ which join smoothly with the present data on a χ vs AGN plot as shown in the Fig. 8. For example, $(Pd_{1-x}Cu_x)_{80+y}P_{20-y}$ alloys (AGN$\approx$ 10) have values of χ which are extremely small ($\sim 10^{-7}$ emu/g G) and of either positive or negative sign depending on composition.[26] The smooth decrease of χ as a function of increasing AGN (for AGN$>$ 6) appears to be a general characteristic of amorphous transition-metal–metalloid alloys. A summary of the present data along with various data from other work are given in Table II. Included are data for the density of states for cystalline $Mo_{61}Ru_{39}$ and $Mo_{42}Re_{58}$ alloys (having the σ-phase structure) as determined from low-temperature specific-heat measurements.

In order to understand the significance of the temperature-independent susceptibility χ, it is necessary to examine the role of various contributions to it. The following procedures are generally used to interpret such data. χ is taken as the sum of two main contributions

$$\chi = \chi_{\text{core}} + \chi_{\text{cond}} , \tag{2}$$

where χ_{core} refers to core electrons and χ_{cond} refers to conduction-band electrons. χ_{cond} naturally divides into contributions from the sp (nearly free) and d (tightly-bound) electrons.

$$\chi_{\text{cond}} = \chi_{sp} + \chi_d . \tag{3}$$

Contributions to χ_{sp} include the Pauli spin term χ_{sp}^P and the Landau term χ_{sp}^L,

$$\chi_{ps} = \chi_{sp}^P + \chi_{sp}^L , \tag{4}$$

while χ_d contains the above two terms plus an orbital term[27]

$$\chi_d = \chi_d^P + \chi_d^L + \chi_d^O . \tag{5}$$

The Pauli spin susceptibility of the sp electrons in the simplest approximation is given by

$$\chi_{sp}^P = 2\mu_B^2 N_{sp}(0) , \tag{6}$$

where $N_{sp}(0)$ is the sp-band density of states (per spin) at the Fermi level and the Landau term for sp electrons is given by

$$\chi_{sp}^L = -\tfrac{1}{3}(m/m^*)\chi_{sp}^P , \tag{7}$$

with m the free electron mass and m^* the actual effective mass for s electrons near E_F. The core term χ_{core} in Eq. (2) and the terms defined by Eqs. (6) and (7) all give contributions to χ which are between one and two orders of magnitude less than the observed values of χ.[28] Thus, the dominant term in χ are χ_d^P and χ_d^O since

$$\chi_d^L = -\tfrac{1}{3}(m/m^*)\chi_d^P \tag{8}$$

and $m^* \gg m$ for d electrons. Thus, χ_d^L is neglected. In the simplest approximation

$$\chi_d^P = 2\mu_B^2 N_d(0) , \tag{9}$$

while the orbial susceptibility χ_d^O is difficult to calculate. χ_d^O is probably less than though comparable with χ_d^P. We shall for the purpose of simplicity assume that χ_d^O does not change with AGN and that χ_d^P is the dominant contribution to χ. In this picture, the variation of χ observed in Fig. 8(b) then reflects mainly the variation of $N_d(0)$ (the density of state per spin) which is roughly given by $\chi_d^P/2\mu_B^2 \approx \chi/2\mu_B^2$. It should be stated that the above discussion ignores many-body effects. The possibility that many-body corrections systematically effect the estimated values of $N_d(0)$ cannot be ruled out.

Finally, the magnetization data taken for $T < T_c$

TABLE II. Magnetic susceptibility at high temperature, corresponding density of states $N(0)$, structure, and AGN of alloys in the present study along with related data for other amorphous alloys and crystalline $Mo_{61}Ru_{39}$ and $Mo_{42}Re_{58}$.

Alloy	Average molecular weight	χ (emu/gG) 10^6	$N(0)$ (states/eV atom spin)	Structure	AGN
$(Mo_{0.8}Ru_{0.2})_{80}P_{20}$	83.8	0.72 ± 0.05	0.93 ± 0.07	amorphous	6.4
$(Mo_{0.6}Ru_{0.4})_{80}P_{20}$	84.6	0.52 ± 0.05	0.68 ± 0.07	amorphous	6.8
$(Mo_{0.4}Ru_{0.6})_{80}P_{20}$	85.4	0.40 ± 0.05	0.53 ± 0.07	amorphous	7.2
$(Mo_{0.2}Ru_{0.8})_{80}P_{20}$	86.2	0.28 ± 0.05	0.37 ± 0.07	amorphous	7.6
$Mo_{80}P_{10}B_{10}$	80.9	0.70 ± 0.05	0.88 ± 0.07	amorphous	6.0
$(Pd_{0.8}Cu_{0.2})_{80}P_{20}$[a]	84.45	0.02 ± 0.005	...	amorphous	10.2
$Pd_{80}P_{20}$[b]	91.3	-0.02 ± 0.005	...	amorphous	10.0
$Mo_{61}Ru_{39}$	...	...	0.87[c]	σ phase	6.8
$Mo_{42}Re_{58}$	...	...	0.70[c]	(crystalline)	

[a] Taken from thesis by G. Tangonan, California Institute of Technology, 1976 (unpublished).
[b] Extrapolated from $(Pd_{1-x}Cu_x)_{80}P_{20}$ data.
[c] From specific-heat data [F. Heiniger, E. Bucher, and J. Müller, Phys. Kond. Mater. 5, 243 (1966)].

show the characteristic M vs H curves of a high-κ type II superconductor. For some samples, irreversibility in the M vs H curve is observed and can be interpreted in terms of flux pinning. These data will be discussed in a separate publication.[25]

IV. DISCUSSION

A. Amorphous-phase formation and stability

The liquid-quenching technique can be used to obtain amorphous alloys which fall into two more or less separate categories.[29] The first, referred to as metal-metalloid alloys consists of a transition metal (TM) alloyed with typically 20 at.% of a nontransition group A element such as phosphorus, silicon, carbon, or boron. The group A element is frequently termed a glass former. The second category of alloys consists of a rare earth, actinide, or early transition metal (e.g., Zr, Ti, etc.) alloyed with a late transition metal (e.g., Rh, Ni, Pd, etc). The common feature of both classes of alloys is the existence of a deep eutectic in the alloy phase diagram near the composition of interest. Turnbull[30] has noted that a deep eutectic can be interpreted in terms of a comparitively large negative heat of formation of the liquid alloy. Since the amorphous structure is closely related to that of the liquid, alloys having compositions near a deep eutectic are prone to amorphous-phase formation.

The alloys of the present study represent an intermediate case between the above two alloy classes. The melting temperature T_m of Mo and Ru are 2610 °C and 2280 °C, respectively. The phase diagram of the Mo-Ru system[31] exhibits a eutectic at the composition $Mo_{58}Ru_{42}$ with a eutectic temperature of 1945 °C. The addition of phosphorus to form the ternary alloy $(Mo_{0.58}Ru_{0.42})_{80}P_{20}$ gives a deep eutectic in the ternary diagram. The liquidus temperature for the ternary alloy is estimated to be ~1400–1800 °C. The estimate is based on observations made during the liquid-quenching process. The Mo-Ru eutectic is the limiting case of a TM-TM eutectic where the separation of the AGN of the TM's is small. For larger separation of the AGN (e.g., the Nb-Rh and Zr-Rh systems[4]) of the TM's, the eutectic is more pronounced. The addition of phosphorus to Mo-Ru alloys lowers the liquidus temperature in a manner characteristic of the metal-metalloid class of amorphous alloys. Use of this ternary alloy is essential for obtaining an amorphous phase by liquid quenching. Attempts to prepare amorphous $Mo_{58}Ru_{42}$, $Mo_{80}P_{20}$, and $Ru_{80}P_{20}$ by liquid quenching were unsuccessful.

Collver and Hammond[6,32] have determined the crystallization temperatures T_{cr} of vapor-quenched transition-metal films. They observed crystallization well below room temperature for pure metal films and most of the alloy films studied. Two notable exceptions to this observation were Nb-Zr and Mo-Ru alloys which were found to have rather high crystallization temperatures. The Mo-Ru alloys, for example, had T_{cr} as high as 700 °C. The crystallization temperature of liquid-quenched amorphous $(Mo_{1-x}Ru_x)_{80}P_{20}$ alloys was found to be of order $T_{cr} \sim 700$–800 °C, very near to that of the Mo-Ru films. It is noteworthy that a number of alloys such as $Nb_{58}Rh_{42}$, $(Mo_{1-x}Ru_x)_{80}P_{20}$,

$Nb_{1-x}Ni_x$,[33] having an AGN (for the transition-metal components) of ~6.5 can be obtained in amorphous form by liquid quenching. These alloys also yield stable amorphous phases when prepared in thin-film form. Based on this observation, it is conjectured that amorphous phase stability (and the existence of a eutectic) can be associated with certain preferred AGN values. Using the Collver Hammond results and those on liquid-quenched alloys, one can determine that alloys having AGN values of ~4.5 and ~6.5 are prone to amorphous-phase formation. It is remarkable that these preferred AGN values coincide with the Matthias preferred AGN values for obtaining high-T_c superconductors. McMillan[34] has shown that enhanced superconductivity in transition metals is typically accompanied by an overall softening of the lattice against harmonic displacements. Gomersall and Gyorffy[35] have discussed the stability of crystalline phases in terms of this effect and have attempted to explain Matthias rules. It is tempting to attribute both lattice softening and the tendency toward amorphous-phase formation to a common origin. Both can be traced to the response of the d electrons to atomic distortion or rearrangement. When the d-electron gas becomes highly polarizable as occurs when the electron-phonon coupling constant is large, one expects that lattice distortion will be energetically easier. In this situation the amorphous phase will have a comparitively lower internal energy with respect to its crystalline counterpart.

B. Upper critical field and electronic properties

Koepke and Bergmann[36] (KB) have measured the upper critical field $H_{c2}(T)$ for amorphous Mo films obtained by low-temperature vapor deposition. They report a linear temperature dependence of H_{c2} in agreement with the present results (Fig. 5). On the other hand, they find an upper critical-field gradient $dH_{c2}(T)/dT \approx 45$ (kG/°K) which is considerably larger than that observed for amorphous $(Mo_{1-x}Ru_x)_{80}P_{20}$ alloys for which $dH_{c2}(T)/dT \sim 24$–28 (kG/°K). It is noteworthy that $dH_{c2}(T)/dT$ is nearly independent of x. For a strong-coupling superconductor, $dH_{c2}(T)/dT$ has been theoretically expressed as[37,38]

$$\frac{dH_{c2}(T)}{dT} = -z\,\frac{4K_B e}{\pi}\,\rho N(0)^*\,, \tag{10}$$

where z is a numerical constant very nearly equal to 1, ρ is the normal-state electrical resistivity of the sample, and $N(0)^*$ is the electron-phonon dressed density of states at the Fermi level ($E_F = 0$). KB have discussed application of Eq. (10) to their results. In the present study, we have observed values of $\rho \sim 300$ $\mu\Omega$ cm while KB found $\rho \sim 450$ $\mu\Omega$ cm for Mo films. For the alloy $(Mo_{0.8}Ru_{0.2})_{80}P_{20}$ we find $T_c = 7.3$ °K, close to that obtained by KB for Mo films. Making the crude assumption that $N(0)^*$ is nearly the same for these two cases, one can account for most of the difference in dH_{c2}/dT by considering the difference in ρ. On the other hand, Eq. (10) does not account for the constancy of dH_{c2}/dT throughout the $(Mo_{1-x}Ru_x)_{80}P_{20}$ alloy series. From the magnetic-susceptibility data (Fig. 8) and the discussion in Sec. III C, it is reasonably clear that $N(0)$ decreases rapidly with increasing Ru concentration. The accompanying rapid decrease in T_c (Fig. 4) implies that the electron phonon coupling constant λ also decreases with increasing Ru concentration. Thus, $N(0)^* = N(0)(1+\lambda)$ must be a rapidly decreasing function of AGN. On the other hand, ρ remains nearly constant (Table I) so that Eq. (10) predicts a significant decrease in dH_{c2}/dT with increasing AGN. As dH_{c2}/dT is experimentally found to be nearly constant, it is concluded that Eq. (10) fails to describe its dependence on AGN. As mentioned by KB, the combined effect of d and s electrons can render Eq. (10) inapplicable since the transport mean free path is determined mainly by s electrons while the superconductivity most probably involves d electrons as will be discussed in Sec. IV C. It should be added that recent tunneling data on amorphous Mo-base alloy films[39,40] suggests that these superconductors are well described by the BCS weak-coupling theory. Previous work[3] on amorphous simple metals has shown them to be strong-coupling superconductors. KB point out that a value $\lambda \approx 2$ is required if Eq. (10) is to predict the correct magnitude of dH_{c2}/dT for amorphous Mo films. In view of the tunneling data, such a large λ seems highly unlikely. The nearly free-electron model on which Eq. (10) is based cannot it appears account for the complex behavior of amorphous transition metals. The role of d electrons must be considered if one is to understand this behavior.

C. Microscopic origin of the variation of T_c

Several attempts have been made to explain the systematic variation of T_c, observed first by Collver and Hammond,[6] for amorphous transition metals of a given series.[7–9] We can use the data obtained in the present study to help to clarify the role of the various microscopic parameters which determine T_c. It is clear from the previous discussion and by comparison of Figs. 4 and 8 that the electronic density of states at the Fermi level $N(0)$ plays a major role in determining the variation of T_c. Evidence that $N(0)$ plays a significant role in the behavior of T_c has also been obtained by ultra-

violet photoemission spectroscopy on amorphous and bcc films of Mo.[41] Though not quantitative, the photoemission studies indicate a loss of d-band structure and an increase in $N(0)$ on passing from bcc crystalline to amorphous Mo. The function $N(E)$, as qualitatively reflected in the photoelectron energy spectrum, is a smoothly varying function of E (for $E < E_F = 0$) for amorphous Mo. The present results compliment this picture. In Fig. 8 the variation with AGN of χ and the corresponding density of states for the $(Mo_{1-x}Ru_x)_{80}P_{20}$ alloy series along with data from $(Pd_{1-x}Cu_x)_{80}P_{20}$ alloys leads to the folowing picutre of the $4d$ band of these alloys. It is assumed that phosphorus makes only a small contribution to $N(0)$ arising from s-p electrons as discussed in Sec. III C. The d-band density of states $N_d(0)$ varies smoothly with d-band occupation following a "bell shaped" curve. This curve exhibits a broad peak at a value of AGN corresponding roughly to a half-filled d band. This variation is in marked contrast to the crystalline density of states which show a series of sharp peaks in $N(0)$ as a function of AGN.[30] It is interesting to compare data for amorphous alloys with data for $Mo_{61}Ru_{39}$ and $Mo_{42}Re_{58}$ crystalline alloys having the σ-phase structure. The σ phase has a complex unit cell containing 30 atoms in five nonequivalent positions, and σ-phase alloys typically exhibit a high degree of atomic disorder. Such a low-symmetry poorly ordered structure might be expected to have an electronic band structure similar to an amorphous phase. The density of states $N(0)$ for the above mentioned σ-phase alloys as deduced from specific-heat data (see Table II) is included in Fig. 8(b). It is observed that these values of $N(0)$ fall on the amorphous $N(0)$ vs AGN curve to within experimental uncertainty. It is noteworthy that the superconducting transition temperatures $T_c = 7.0$ and 8.4 °K (respectively, for $Mo_{61}Ru_{39}$ and $Mo_{42}Re_{58}$) also fall close to those observed in the amorphous alloys having the same AGN. Although this close agreement in Fig. 8(b) may be fortuitous, it provides evidence that the density of states deduced from the magnetic-susceptibility data is a meaningful quantity. It is reasonable to proceed by assuming that the variation of $N_d(0)$ is well represented by the dashed curve in Fig. 8(b). The consequences of such a d-band structure for the microscopic theory of electron-phonon interactions and superconductivity are now examined.

McMillan[30] has shown that the superconducting transition temperature can be related to several microscopic parameters through the following equation:

$$T_c = \Theta_D/1.45 \exp\left(\frac{-1.04(1+\lambda)}{\lambda - \mu^*(1+0.62\lambda)}\right), \tag{11}$$

where Θ_D is the Debye temperature (or a suitably defined average phonon frequency), λ is the electron-phonon coupling constant which may be expressed in the form

$$\lambda = N(0)\langle I^2\rangle / M\langle\omega^2\rangle \tag{12}$$

and μ^* represents the Coulomb interaction. In the expression for λ, $\langle I^2\rangle$ is an average of the squared electron-phonon matrix element, M the ionic mass, and $\langle\omega^2\rangle$ an average square phonon frequency. The tight-binding approximation has been shown to give a successful description of superconductivity in d-band metals.[10,11] Labbé, Barasic, and Friedel[10] were the first to point out that simple relationships among the parameters of Eq. (12) follow from a tight-binding model. A simple tight-binding picture predicts the approximate constancy of the product $N(0)\langle I^2\rangle$ by the relationship

$$N(0)\langle I^2\rangle \simeq q_0^2 E_c\ , \tag{13}$$

where q_0 is the Slater coefficient for exponential decay of a d orbital and E_c the principal d-band contribution to cohesive energy. Varma and Dynes[11] extended this picutre to include nonorthogonality of the basis functions as parameterized by the overlap integral S. They derive the interesting approximate relationship

$$\frac{\langle I^2\rangle}{M\langle\omega^2\rangle} \simeq \frac{(1+S)[1+N(0)W(1\mp S)]}{N(0)} \simeq W(1\mp S)\,, \tag{14}$$

where W is the width of the d band, and the upper and lower signs refer to the lower and upper half of the d band, respectively. We can take these results as a rough guide to interpreting the present data in the context of the tight-binding approximation. We assume that the Fermi level lies in the nonbonding (upper half) of the d band for the series of alloys in the present work as the alloys fall in the range of AGN greater than 6. The positive sign is then appropriate. A rigid-band picture implies that the bandwidth W is roughly constant for our alloy series. S is taken to be constant as the Slater coefficient q_0 of the d orbitals for Mo and Ru will be nearly equal,[10] and the mean interatomic distance between neighboring atoms does not change with composition.[42] Equations (12) and (14) then predict that the electron phonon coupling constant λ is proportional to $N(0)$. We can compare this prediction to the present experimental results by assuming that the density of states curve of Fig. 8(b) accurately represents the variation of $N_d(0)$ with AGN. As previously discussed, we ignore the role of phosphorous in determining $N_d(0)$ as the d levels of phosphorus all

lie well above the Fermi energy of the alloy and are not involved in superconductivity. Hybridization effects are also ignored within the spirit of the Varma-Dynes model.

The experimentally observed decrease in T_c with increasing AGN (Fig. 4) is then seen to be governed mainly by the variation of $N_d(0)$. Quantitative comparison requires that we deduce λ from T_c using the McMillan equation [Eq. (11)]. To do this, a knowledge of the variation of Θ_D is required. As no specific-heat, neutron-scattering, or tunneling data are yet available, one can only speculate as to the variation of Θ_D and the details of the phonon spectrum. A few somewhat quantitative statements can be made. First, if $N_d(0)$ decreases as rapidly with increasing AGN as indicated by Fig. 8(b), then the corresponding decrease in λ predicted by Eq. (14) would result in a more rapid decrease of T_c than experimentally observed if it were assumed that Θ_D does not change with AGN. If the Varma-Dynes picture is to give a quantitative account of the data, then Θ_D must also increase with increasing Ru concentration. The required increase of Θ_D would be of the order of 50% or more on going Mo-rich to Ru-rich alloys. Although this seems unlikely, it should be observed that $\Theta_D = 460$ and 550 °K for the pure metals Mo and Ru, respectively. This variation is in the right direction required by the Varma-Dynes model. Considering the approximate nature of the model, it can be said that the data are at least qualitatively consistent with it. More detailed analysis must await further data from low-temperature specific-heat measurements. Such measurements are currently in progress in this lab and should both confirm the variation of $N(0)$ deduced from the magnetic susceptibility data as well as give additional information on the variation of Θ_D. It is expected that a detailed understanding of the variation of the microscopic parameters which govern T_c in amorphous transition metals and alloys can be obtained. This information should be very useful in understanding the systematics of superconductivity in crystalline transition-metal alloys as well.

V. SUMMARY

It has been demonstrated that alloys based on the $4d$-transition metals Mo and Ru may be obtained in amorphous form using the technique of rapid cooling from the liquid state. The amorphous phases so obtained are stable up to temperatures of 700–800 °C. The structure of these materials has been investigated both by x-ray and transmission electron diffraction techniques and found to be similar to that of other amorphous alloys for which radial distribution functions have been computed. Superconductivity has been observed in all of these alloys. The transition temperatures of the alloys follow a systematic behavior (with the AGN of the transition-metal constituents) closely resembling that observed by Collver and Hammond for vapor-quenched transition-metal films.

The upper critical field H_{c2} depends linearly on temperature and is characterized by a large gradient $dH_{c2}/dT \sim 25$–30 kG/°K for all alloys of the series. This temperature dependence is not well described by the theories of Maki or Werthameter. The values of the gradient were compared with a theoretical expression derived by Rainer, Bergmann, and Eckhardt. This expression does not account for either the magnitude or the composition dependence of the gradient.

Magnetization measurements as a function of temperature show that it is possible to determine the temperature-independent contribution to the normal-state magnetic susceptibility of the alloys. The Pauli paramagnetic contribution can be estimated and used to give an estimate of the electronic density of states at the Fermi level $N(0)$. It is found that the estimated $N(0)$ values decrease systematically with increasing AGN of the transition-metal constituent. This variation can be correlated with the variation in T_c. Several relationships derived by Varma and Dynes based on the tight-binding approximation for the d band of transition-metal alloys are compared with the present data and are found to be in qualitative agreement with it. It was pointed out that additional information from specific-heat measurements will be required if one is to understand the microscopic origin of the variation in T_c in detail. Superconductive tunneling experiments would also be of great value in providing information concerning the microscopic parameters which govern superconductivity. By understanding superconductivity in amorphous transition metals, one might hope to obtain a better understanding of crystalline transition-metal alloys. Long-range structural order in crystalline superconductors can perhaps be considered to result in a refinement of a basic model for electronic structure which emphasizes the local coordination and short-range order present in both the crystalline and amorphous state.

ACKNOWLEDGMENT

The authors wish to thank Art Williams for assistance with the experimental work and Sumio Kotake for technical assistance. This work was supported by Department of Energy, Contract No. EY-76-C-03-0822.

*Present address: W. W. Hansen Laboratories of Physics, Standford University, Standford, Calif. 94305.
†Present address: Laboratoire de Structure Electronique des Solides, European Research Associates 100, 4 Rue Blaise Pascal, 67000 Strasbourg, France.

[1]W. Buckel and R. Hilsch, Z. Phys. 138, 109 (1954).
[2]W. Buckel and R. Hilsch, Z. Phys. 138, 118 (1954).
[3]G. Bergmann, Phys. Rep. 27, 159 (1976).
[4]W. L. Johnson, S. J. Poon, and P. Duwez, Phys. Rev. B 11, 150 (1975); W. L. Johnson and S. J. Poon, J. Appl. Phys. 46, 1787 (1975).
[5]W. H. Shull and D. G. Naugle, Bull. Am. Phys. Soc., 22, 403 (1977).
[6]M. M. Collver and R. H. Hammond, Phys. Rev. Lett. 30, 92 (1973).
[7]G. Kerker and K. H. Bennemann, Z. Phys. 264, 15 (1973).
[8]G. Kecker and K. H. Bennemann, Solid State Commun. 14, 399 (1974).
[9]R. H. Hammond and M. M. Collver, Low Temp. Phys. 3, 532 (1974).
[10]S. Barasic, J. Labbé, and J. Friedel, Phys. Rev. Lett. 25, 919 (1970).
[11]C. M. Varma and R. C. Dynes in *Superconductivity in d and f band Metals*, edited by D. H. Douglass (Plenum, New York, 1976).
[12]P. Duwez, *Progress in Solid State Chemistry*, (Pergamon, Oxford, 1966), Vol. 3.
[13]G. S. Cargill III, J. Appl. Phys. 41, 12 (1970).
[14]G. S. Cargill III and R. W. Cochrane, J. Phys. (Paris) 35 C4-269 (1974).
[15]C. N. J. Wagner, J. Vac. Sci. Technol. 6, 650 (1969).
[16]O. Meyer, *New Uses of Ion Accelerators*, edited by J. F. Ziegler (Plenum, New York, 1975), p. 323.
[17]O. Meyer, *Application of Ion Beams to Materials*, Inst. Phys. Conf. Ser. 28, 168 (1976).
[18]W. L. Johnson and C. C. Tsuei, Phys. Rev. B 13, 4827 (1976).
[19]W. L. Johnson, C. C. Tsuei, and P. Chaudhari Phys. Rev. (to be published).
[20]K. Togano and K. Tachikawa, Phys. Lett. A 54, 205 (1975).
[21]B. G. Lazarev, L. S. Lazareva, E. E. Semenenko, V. I. Tutov, and S. I. Goridov, Sov. Phys.-Dokl. 16, 147 (1971).
[22]W. L. Johnson and S. J. Poon, IEEE Trans. Magn. 11, 189 (1975).
[23]V. M. Kuz'Menco, V. G. Lazarev, V. I. Mel'Nikov, A. I. Sudoftsov, Zh. Eksp. Teor. Fiz. 67, 801 (1974). [Sov. Phys.-JETP 40, 396 (1974).
[24]K. Maki, Physics (N.Y.) 1, 127 (1964); K. Maki, Phys. Rev. 148, 362 (1966); N. R. Werthamer, E. Helfand, and P. C. Hohenberg, Phys. Rev. 147, 288 (1966).
[25]W. L. Johnson and S. J. Poon (unpublished).
[26]G. Tangonan, PhD. thesis, (California Institute of Technology, 1976) (unpublished).
[27]R. Kubo and Y. Obata, J. Phys. Soc. Jpn. 11, 547 (1956).
[28]A. M. Clogston, V. Jaccarino, and Y. Yafet, Phys. Rev. 134, A650, (1964); F. I. Ajami, R. K. MacCrone, J. Phys. Chem. Solids 36, 7 (1975).
[29]P. Duwez, Ann. Rev. Mater. Sci. 6, 83 (1976).
[30]D. Turnbull, J. Phys. (Paris) Colloq. 35, 1 (1974).
[31]R. P. Elliot, *Constitution of Binary Alloys* (McGraw-Hill, New York, 1965), Suppl. 1.
[32]M. M. Collver and R. H. Hammond, (private communication).
[33]R. C. Ruhl, B. C. Giessen, M. Cohen, and N. J. Grant, Acta Metall. 15, 1693 (1967).
[34]W. L. McMillan, Phys. Rev. 167, 331 (1968).
[35]L. R. Gomersall and B. L. Gyorffy, Phys. Rev. Lett. 33, 1286 (1974).
[36]R. Koepke and G. Bergmann, Solid State Commun. 19, 435 (1976).
[37]G. Eilenberger and V. Ambegaokar, Phys. Rev. 168, 332 (1967).
[38]D. Rainer, G. Bergmann, and U. Eckhardt, Phys. Rev. B 8, 5324 (1973).
[39]C. C. Tsuei, W. L. Johnson, and R. L. Laibowitz, Bull. Am. Phys. Soc. 22, 289 (1977); Solid State Commun. (to be published).
[40]W. L. Johnson, C. C. Tsuei, S. I. Raider, and R. L. Laibowitz (unpublished).
[41]B. Schroeder, W. L. Johnson, C. C. Tsuei, P. Chaudhari, and J. Gradzyk, AIP Conf. Proc. 31, 353 (1976); B. Schroeder, W. Grobman, W. L. Johnson, C. C. Tsuei, and P. Chaudhari, *Proceedings of the Fourth International Conference on the Physics of Noncrystalline Solids*, edited by G. H. Frishchat, Trans. Tech., Aedermannsdorf, Switzerland, 1977), p. 190—195.
[42]The metallic radii of Mo and Ru are 1.36 and 1.30 Å, respectively, and thus the nearest-neighbor distance should not change significantly with composition. The position of the first maximum in the x-ray intensity function does not change appreciably with composition lending experimental support to this contention.

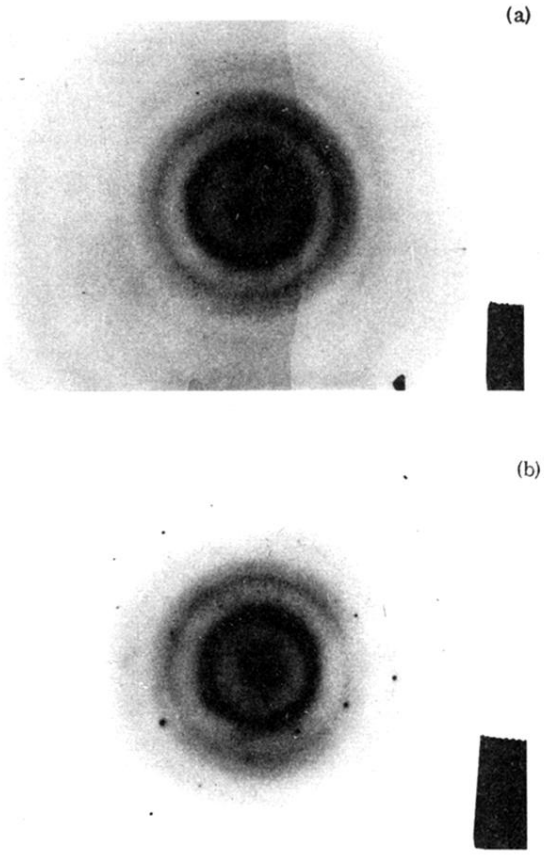

FIG. 2. (a) Transmission-electron diffraction pattern for a typical region of an amorphous $(Mo_{0.6}Ru_{0.4})_{80}P_{20}$ sample. The foil was thinned by chemical etching; (b) Transmission-electron diffraction pattern of a region of a $(Mo_{0.2}Ru_{0.8})_{80}P_{20}$ specimen containing a microcrystallite embedded in an amorphous matrix. Most regions of this sample showed no evidence of crystallization.